Teraguchi, Hiroshi; Nakagawa, Hajime; Zhang, Hao

Study on Flow and Bed Deformation around Impermeable and Permeable Groins

STUDY ON FLOW AND BED DEFORMATION AROUND IMPERMEABLE AND PERMEABLE GROINS

Hiroshi Teraguchi[1], Hajime Nakagawa[2] and Hao Zhang[3]

[1] Graduate Student, Department of Civil and Earth Resources Engineering, Kyoto University
Katsura Campus, Nishikyo-ku, Kyoto 615-5840, Japan, e-mail: teraguchi@uh31.dpri.kyoto-u.ac.jp
[2] Professor, Disaster Prevention Research Institute, Kyoto University
Shimomisu, Yoko-Oji, Fushimi-ku, Kyoto, 612-8235, Japan, e-mail: nakagawa@uh31.dpri.kyoto-u.ac.jp
[3] Assistant Professor, Disaster Prevention Research Institute, Kyoto University
Shimomisu, Yoko-Oji, Fushimi-ku, Kyoto, 612-8235, Japan, e-mail: zhang@uh31.dpri.kyoto-u.ac.jp

ABSTRACT

Groins are river management structures designed to protect riverbanks from erosion or to provide enough flow depth for navigation purposes. Nowadays, groins are also constructed in channels for the preservation and maintenance of ecosystems because diversified flow around groins creates conditions suitable for riverbank vegetation and aquatic biota. This research presents the results obtained from the experimental and numerical studies on turbulent flow and bed deformation around groins. A pair of impermeable and permeable groins was positioned on the left side of a model channel. The velocity distributions and bed deformation were measured around the pair of impermeable or permeable groins under non-submerged condition. The resulted local scour hole around the first groin in the impermeable case was deeper than that in the permeable case. The velocity distributions showed the influence of each type of groin on the flow field. A 3D numerical model based on unstructured meshes was developed to simulate the flow field around the groins in scoured bed conditions. The results of the numerical model were compared with those of the experimental measurements.

Keywords: groins, non-submerged, permeable, 3D numerical model, unstructured meshes

1. INTRODUCTION

The influence on water flow and sediment transport caused by river structures has been carried out during the years. One type of river structures are groins that have been widely used to redirect the flow in channels and to protect eroding streams banks (Copeland, 1983; Maza Alvarez, 1990; Uijttewaal, 2005). Nowadays, groins are also constructed in rivers for the preservation and maintenance of ecosystems because diversified flow around groins creates conditions suitable for riverbank vegetation and aquatic biota (Klingeman et al., 1984; Carling et al., 1996).

According to the permeability of the structure, groins are classified into two types: impermeable ones and permeable ones. The first type is generally constructed using local rocks, gravels or gabions and the second one consists of rows of piles, bamboo or timbers (Klaassen, 2002). The two types of groins affect the flow field and sediment transport in different ways and result in various flow patterns and bed morphologies (Zhang, 2005; Zhang et al., 2006). However, the hydraulic and morphological impacts of groins are not completely understood. In some cases, the local scour at the toes of the groins and the deposition in the main channel are unwanted with respect to the stability of the groin structure and the effectiveness of channel width for the purpose of navigation (Gill, 1972). In other cases, this

kind of structures can cause impacts in fish's habitat as the reduction in the number of fishes or causing its migration to other places. For a better understanding of the flow and/or bed deformation in groin fields, many studies have been conducted in case of single groin (Kuhnle, 2002). However, in practice, groins are usually organized in a group, so a lot of studies are still needed.

In this study, the flow and local scour around two impermeable or permeable groins was investigated through the laboratory experiments and numerical simulations. Experiments are able to provide reliable information under specific and controlled conditions. The similarities in process as flow separation and the formation of vortices will allow another generic application for validate modelling tools. In view of these, a 3D numerical model based on unstructured meshes was developed. The simulated results were compared with experimental results.

2. LABORATORY EXPERIMENT

Experimental study was carried out in a physical model constructed in Ujigawa Open Laboratory, Disaster Prevention Research Institute, Kyoto University. This model consists of a straight flume of 10m-long, 0.80m-wide and 0.28m-deep (0.45m-deep in test region). For all experiments, the bed slope of the channel was adjusted to 1/800. The detailed sketch of the experimental set-up is shown in Figure 1.

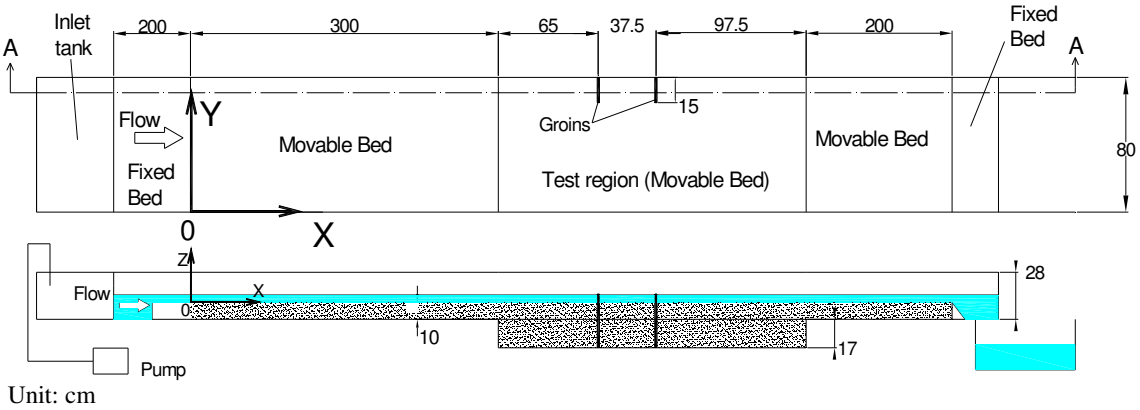

Figure 1 Experimental set-up (top view, top; longitudinal view (section A-A),bottom,not to scale)

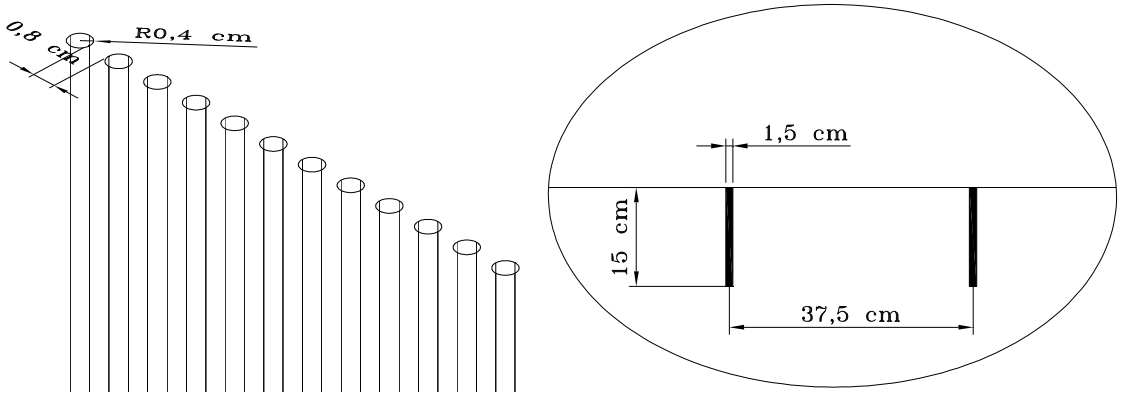

Figure 2 Details of permeable groin (left side) and groins geometry (right side).

The x-axis starts from the upstream end of the movable bed, the y-axis from the right wall of the flume and the z-axis from the initial flat bed level. There is a fixed bed, made of wooden plank elevated 10cm above the bottom at the upstream entrance. The function of the wooden plank is to smoothen the flow. Two groins are placed perpendicular to the channel banks on the left side of the flume in the test region (Figure 2 - right). In Case 1, impermeable groins, made of wooden cuboids, are used. In Case 2, permeable groins (Figure 2 - left), made with a series of round sticks, are designed to have a permeability of 50%. The sediment utilized is coal (powdered anthracite) with a mean diameter of 0.83mm and a specific gravity of 1.41g/cm^3.

The experiments are conducted under uniform flow conditions. The hydraulic parameters adopted for these experiments are given in Table 1. Uniform flow condition is established by adjusting the tailgate height of the flume. Constant rate of sediment is supplied continuously from the upstream boundary of the flume to maintain the dynamic equilibrium state. The dry sediment is mixed with water before it is supplied in order to avoid the dispersion effects. The sediment transport rate is evaluated with the bed load transport formula proposed by Ashida-Michiue (1972), but the amount of sediment was finally adjusted after some trial experiments. Five hours duration for each experiment are found sufficient for the attainment of dynamic equilibrium condition.

Table 1 Details of the experimental conditions

Discharge Q(l/s)	6.50	Friction velocity ratio u^*/u^*_c	1.91
Mean velocity u(cm/s)	20.31	Reynolds number, Re	6,202
Flow depth h(cm)	4.00	Froude number, Fr	0.324
Friction velocity u^*(cm/s)	2.22	w_o / u^*	1.829

w_o= sediment settling velocity

At the downstream boundary, a tailgate is used to control the water level. The water level is measured with a point gauge installed on a measuring carriage and the bed deformation is obtained through a laser sensor after the flume has been completely drained out.

For the measurement of velocity field, cements are used to fix the final bed deformation form. After fixing the bed, the same discharge is imposed to measure the flow velocities around the groins using two electromagnetic velocimeters, one with an I-shape sensor (measurements in X-Y plane) and another with an L-shape sensor (measurements in X-Z and Y-Z planes). Considering the bed roughness effects there is no difference between cements and sediments (coal) that could cause changes in the velocity results.

3. NUMERICAL MODEL

For the time being, the numerical model is used to simulate the flow field based on fixed-bed conditions. The governing equations of proposed numerical model are based on the steady 3D RANS (Reynolds-averaged Navier-Stokes equations) and the continuity equation, which can be expressed in a Cartesian coordinate system with the tensor notation as follows.

$$u_j \frac{\partial u_i}{\partial u_j} = F_i - \frac{1}{\rho}\frac{\partial p}{\partial x_i} + \nu \frac{\partial^2 u_i}{\partial x_j \partial x_j} + \frac{1}{\rho}\frac{\partial \tau_{ij}}{\partial x_i} \tag{1}$$

$$\frac{\partial u_i}{\partial x_i} = 0 \tag{2}$$

where u_i= time-averaged velocity; x_i= Cartesian coordinate component; ρ = density of the fluid; F_i= body force; p= time-averaged pressure; ν= molecular kinematic viscosity of the fluid; $\tau_{ij} = -\rho u_i' u_j'$, are the Reynolds stress tensors, and u_i' is the fluctuating velocity component.

The standard k-ε model is used for the turbulence closure. The Reynolds tensors are acquired through the linear constitutive equation.

$$-\overline{u_i' u_j'} = 2\nu_t S_{ij} - \frac{2}{3}k\delta_{ij} \tag{3}$$

where k= turbulence kinetic energy; δ_{ij} = the Kronecker delta; ν_t = eddy viscosity and S_{ij}= the strain-rate tensor, the latter three are expressed by

$$\delta_{ij} = \begin{cases} 1 & if \quad i = j \\ 0 & if \quad i \neq j \end{cases} \tag{4}$$

$$\nu_t = C_\mu \frac{k^2}{\varepsilon} \tag{5}$$

$$S_{ij} = \frac{1}{2}\left(\frac{\partial u_i}{\partial x_j} + \frac{\partial u_j}{\partial x_i}\right) \tag{6}$$

in which C_μ is a coefficient, and is set to be a constant and equal to 0.09, ε is the dissipation rate of the turbulence kinetic energy k.

Two transport equations as described below are employed to estimate k and ε, respectively.

$$u_j \frac{\partial \kappa}{\partial x_j} = \frac{\partial}{\partial x_j}\left(\nu + \frac{\nu_t}{\sigma_\kappa}\frac{\partial \kappa}{\partial x_j}\right) + G - \varepsilon \tag{7}$$

$$u_j \frac{\partial \varepsilon}{\partial x_j} = \frac{\partial}{\partial x_j}\left(\nu + \frac{\nu_t}{\sigma_\varepsilon}\frac{\partial \varepsilon}{\partial x_j}\right) + \left(c_{\varepsilon 1} G - c_{\varepsilon 2}\right)\frac{\varepsilon}{\kappa} \tag{8}$$

where G= the rate-of-production of the turbulence kinetic energy k, is defined as

$$G = -\overline{u_i' u_j'}\frac{\partial u_i}{\partial x_j} \tag{9}$$

and the model constants are used as suggested by Rodi (1980) Zhang et al. (2006b) give a detailed presentation about the numerical schemes, discretization methods, solution methods, equation solvers and the convergence criteria

In the simulation, the inlet boundary is considered as a Dirichlet boundary and all the quantities are prescribed. The outlet boundary has been set far from the groin area, a Neumann boundary with zero gradients is assumed there. The wall function approach is adopted near impermeable boundaries. The permeable groin is expressed as a cluster of

impermeable groins and each permeable groin is expressed with some fine meshes in the simulation.

The simulation sequence follows the SIMPLE (Semi-implicit method for pressure-linked equations) procedure. At first, the momentum equations are solved for each velocity components, in which the pressure, the eddy viscosity, the turbulent kinetic energy and its dissipation rate are considered as known. The resultant velocity field is used to calculate the mass fluxes through faces of Control Volumes. After the pressure correction equation is solved, the velocity field is improved. Finally, the transport equations for the turbulent kinetic energy and its dissipation rate are solved and the eddy viscosity is updated.

The above procedures are repeated until the residual level becomes sufficiently small or the prescribed maximum iteration step number is covered.

4. RESULTS AND DISCUSSIONS

(1) Experimental results

The bed deformations at equilibrium condition in both cases are shown in Figure 3. It can be seen that the erosion around the upstream groin in Case 1 (impermeable groins) is deeper and larger than that in Case 2 (permeable groins). The maximum depths of scour hole around the upstream groin in Case 1 and 2 reach about 15cm and 2cm, respectively. The deposition area in Case 1 is concentrated in the downstream region of the downstream groin due to the reduction of the velocity and recirculation flows occurring in this region. On the other hand, in Case 2, the deposition area is distributed throughout the channel with a small concentration downstream of the downstream groin. This difference occurs due to the permeability of the groins, while in Case 1 the reduction of velocity and the recirculation of flow around the groins are bigger comparing to the Case 2.

The longitudinal profiles of water level and bed level along the channel (y=40cm and y=72cm) in Cases 1 and 2 are shown in Figures 4, 5, 6 and 7, respectively.

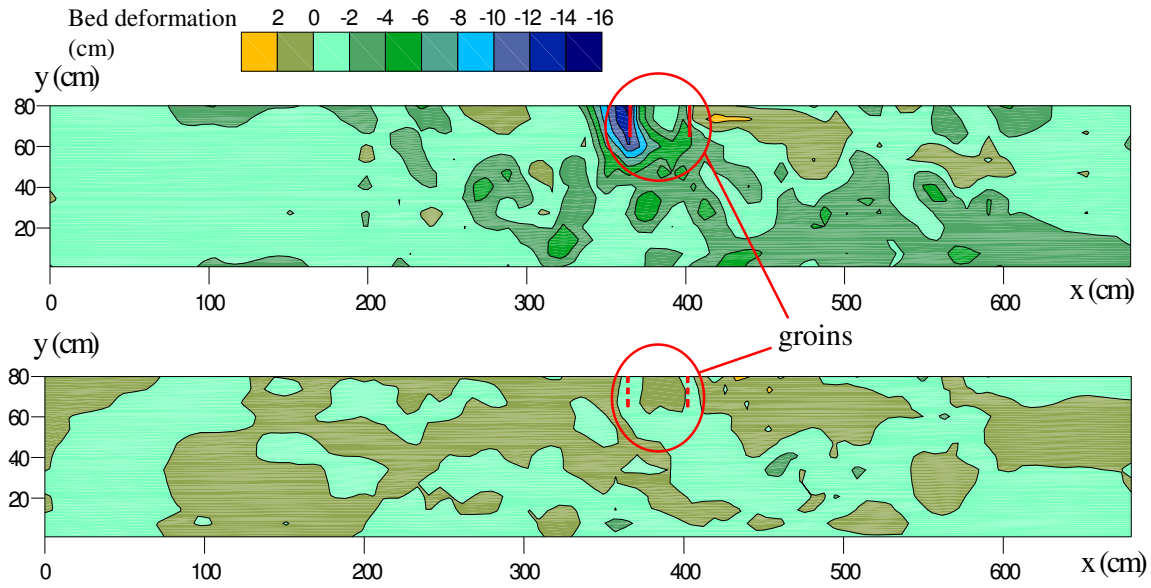

Figure 3 Bed contours at equilibrium condition (top: Case 1 (impermeable groins); bottom: Case 2 (permeable groins))

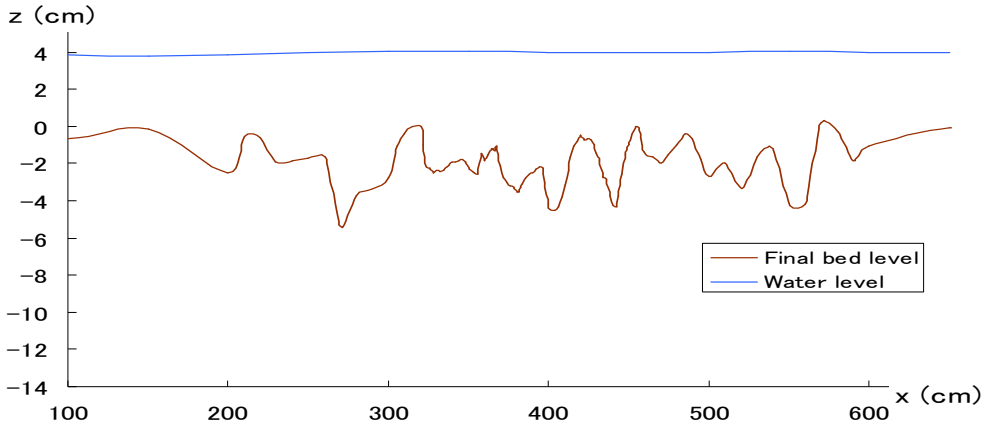

Figure 4 Longitudinal profile of water surface and bed level along main channel (y=40cm) – Case 1.

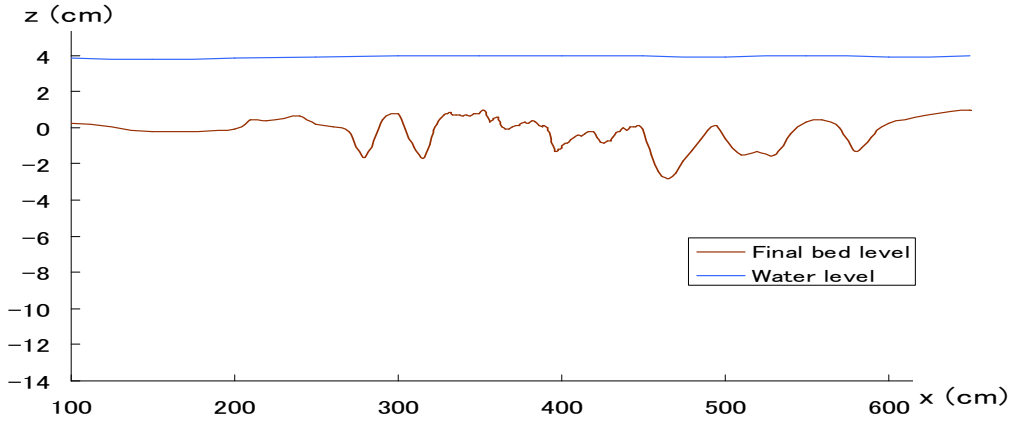

Figure 5 Longitudinal profile of water surface and bed level along main channel (y=40cm) – Case 2.

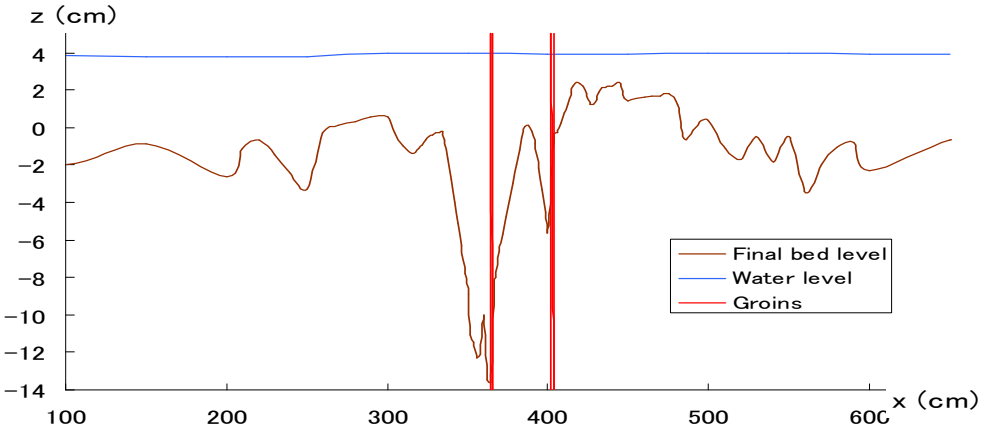

Figure 6 Longitudinal profile of water surface and bed level along channel (y=72cm) – Case 1

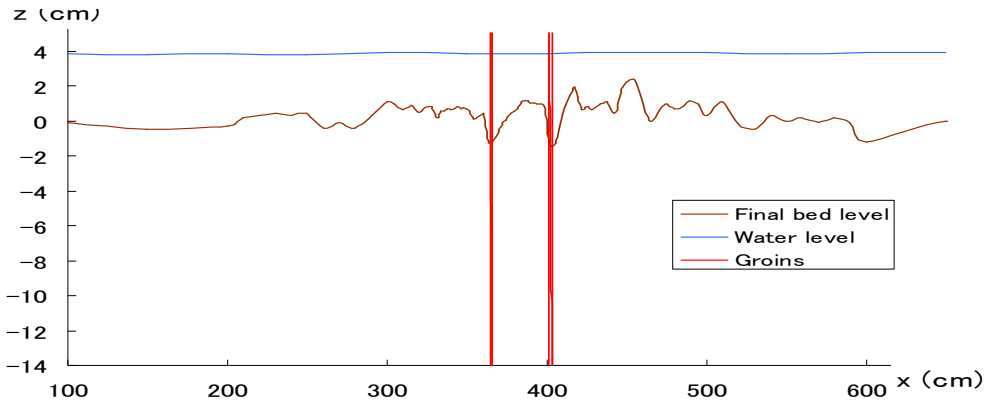

Figure 7 Longitudinal profile of water surface and bed level along channel (y=72cm) – Case 2

The level z=0cm denotes the initial flat bed level. The longitudinal section y=40cm corresponds to the centerline of the flume and y=72cm corresponds to the longitudinal section 8cm from the left wall of the channel and passing through the groins region. In both cases, a small increase of the water level near the groins can be seen, probably due to the effects of the contraction of the flow width by groins. The erosion depth around the groins in Case 1 can be seen with details in Figure 6.

(2) Comparison of numerical and experimental results

Numerical results of flow velocity are compared with those of measured ones based on the deformed fixed bed around groins of Case 1 and 2.

a) Velocity distribution around the impermeable groins in XY plane – Case 1 (z=2.0 cm)

The velocity distributions of experimental and simulated results around impermeable groins on the level of z=2.0cm are shown in Figure 8 and Figure 9, respectively. The magnitude of the simulated velocity agrees well with that of the experiment. When the flow approaches the upstream groin, major part of the obstructed flow diverts to the main channel, which creates a mixing zone in front of the groin head. A part of the flow travels downstream which creates recirculation flow between the groins.

Comparing the simulation results with the experimental ones, the flow structures are quite similar in the upstream area of the groins but differ to some extent in the downstream area. A clear recirculation flow is observed in the simulation results comparing with the experimental results. One reason may be the measurement grid is too coarse for the experiment.

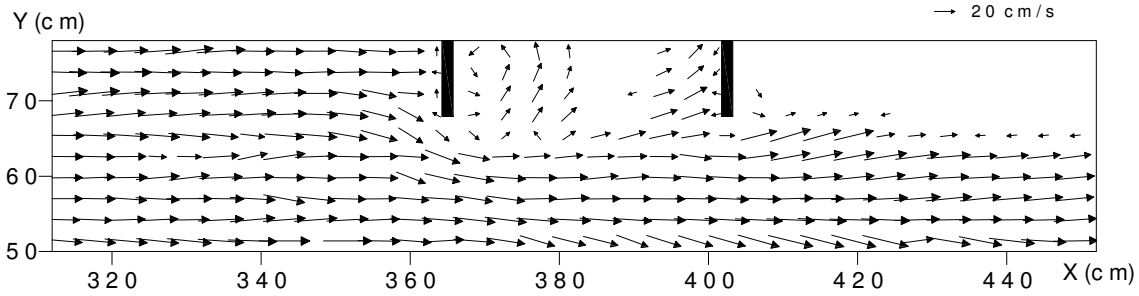

Figure 8 Velocity field around groins in XY plane at z=2.0cm – Case 1 (experiment).

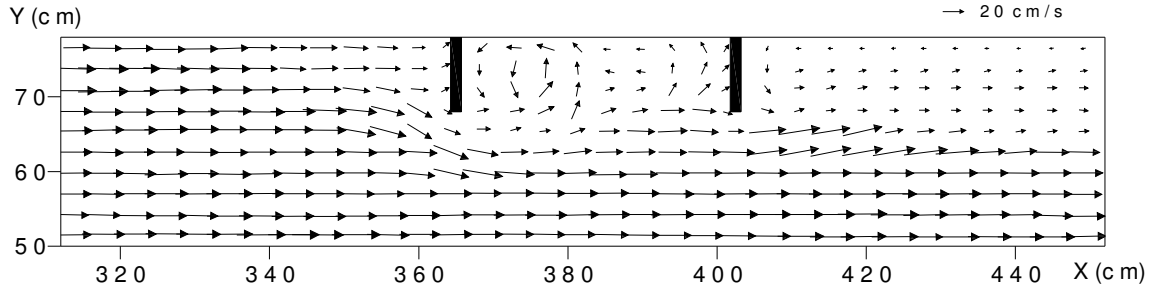

Figure 9 Velocity field around groins in XY plane at z=2.0cm – Case 1 (simulation).

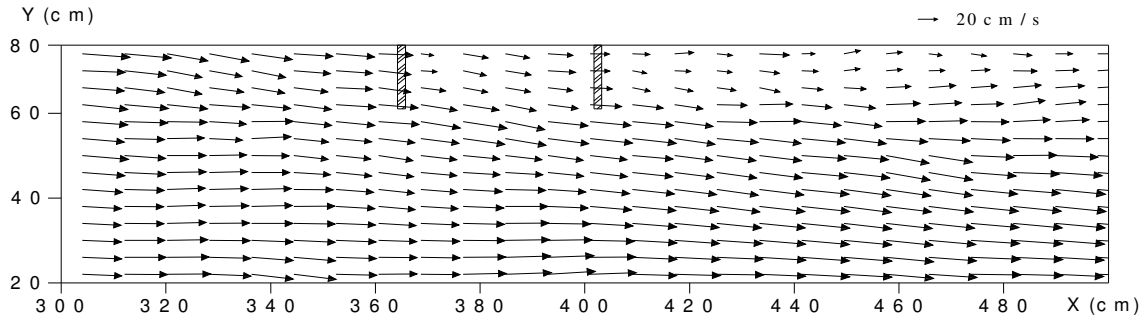

Figure 10 Velocity field around groins in XY plane at z=2.0cm – Case 2 (experiment).

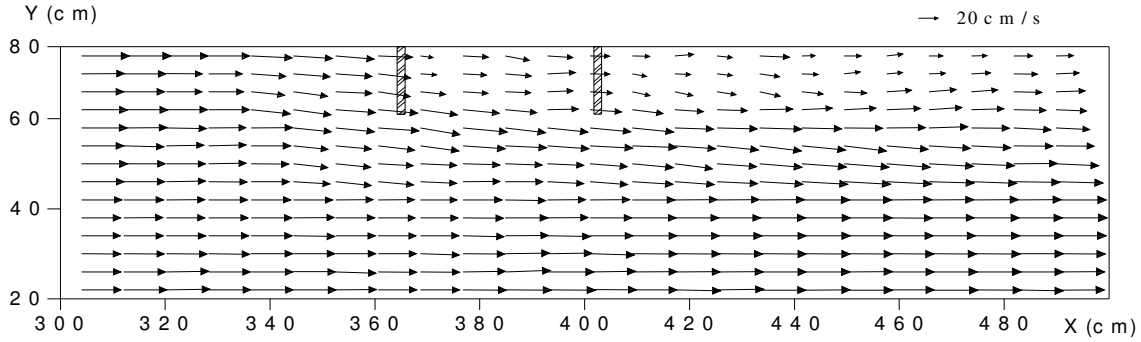

Figure 11 Velocity field around groins in XY plane at z=2.0cm – Case 2 (simulation).

b) Velocity distribution around permeable groins in XY plane – Case 2 (z=2.0cm)

For the permeable groins, the velocity fields around the groins of experimental and simulated results are shown in Figure 10 and Figure 11, respectively.

In this case, the flow directions are not greatly changed. It can be seen that just after passing the upstream groin, the flow direction diverts to the right side wall in the experimental results. At the downstream of the upstream groin, reduction of velocity occurs, but after the flow passed the downstream groin the reduction becomes more significant. The sediment deposition observed downstream of the downstream groin (see Figure 3 bottom) could be caused by this velocity reduction.

Compared with Case 1 (impermeable groins), the flow patterns in Case 2 show practically parallel to the channel near the groins head.

c) Velocity distribution near the upstream groin in YZ plane – Case 1

The velocity vectors in YZ plane near the upstream groin of experimental and simulation results in Case 1 are shown in Figure 12 and Figure 13, respectively.

The longitudinal position of this cross section is x=362cm, just 2.25cm upstream of the upstream groin, seen from downstream to upstream.

From the experimental results, the recirculation flow near the upstream groin is quite similar to the computed results. The bed erosion around the upstream groin probably results from the influence of this recirculation flow that is more evident near the groin (from y=65cm to y=80cm). It means the flow is attacking the channel bank and can cause the erosion in this region. Hence, bank protection measures are needed when this kind of groin is utilized.

The velocity vectors in Case 2 with permeable groin is not shown here because the flow passing through the piles causes only a small recirculation upstream of the upstream groin and without causing significant erosion around the groins (see Figure 7) compared with the case of impermeable groins (see Figure 3 bottom).

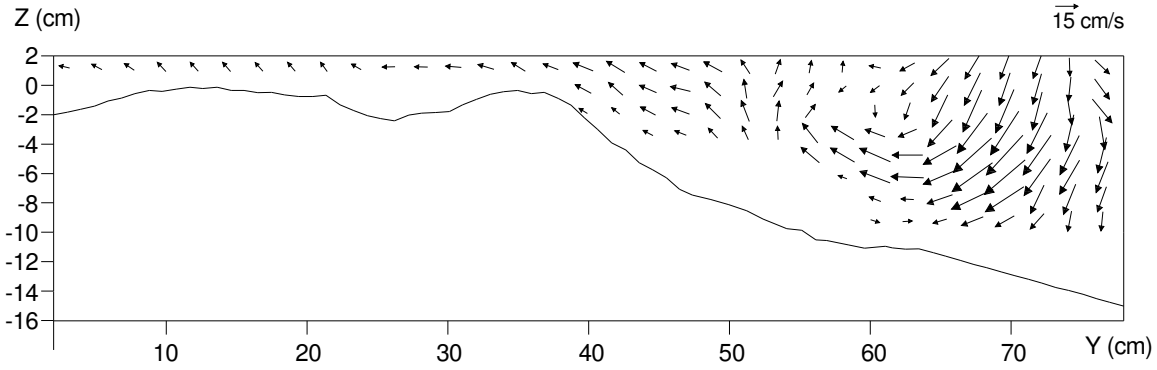

Figure 12 Velocity field around groins in YZ plane at x=362cm – Case 1 (experiment).

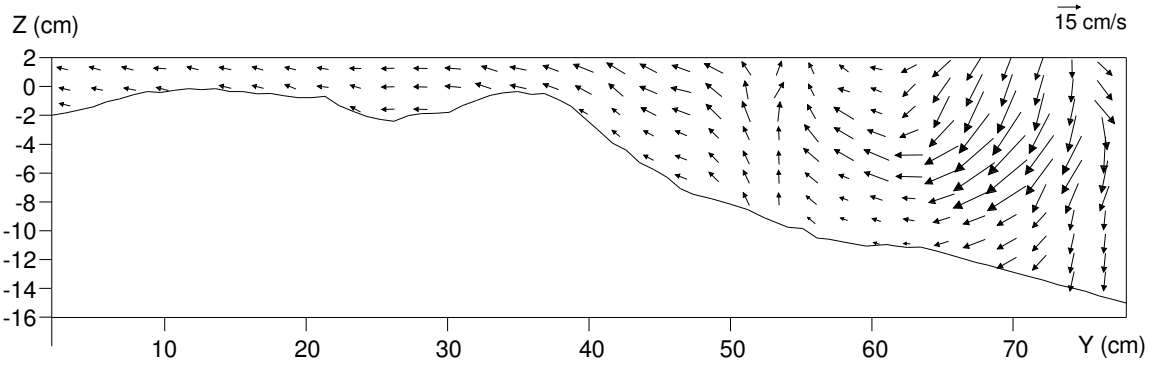

Figure 13 Velocity field around groins in YZ plane at x=362cm – Case 1 (simulation).

5. CONCLUSIONS

This study analyzed the effects on flow pattern and bed deformation due to the presence of impermeable or permeable groins in experimental flume under non-submerged

scour condition.

Experimental result indicates the influence of the groins permeability on the bed deformation and flow structures around groins. In the same hydraulic conditions, the erosion around the upstream groin is significantly deep in the case of impermeable groins (Case 1) compared with the case of permeable groins (Case 2). The velocity field in the impermeable case showed the influence of groins because the separation of the flow, partly to the main channel and partly to the sidewall direction causing the recirculation of the flow in this area. In the permeable case the separation is not so evident and the reduction of velocity after the downstream groin is smaller than impermeable case.

The developed numerical model can simulate the flow structures around groins quite reasonably in fixed bed conditions, i.e., using final scoured bed form. In the future works, are expected more 3D simulations to validate the applicability of the numerical model in other cases such as movable bed and/or submerged conditions. The model should also be compared with field data where the results depend on the different conditions that are not considered in this study.

REFERENCES

Ashida, K. and Michiue, M. (1972), Studies on bed load transportation for nonuniform sediment and river bed variation, Disaster Prevention Research Institute Annuals, Kyoto University, No. 14B, pp. 259-273 (in Japanese).

Carling, P. A., Kohmann, F., and Golz, E. (1996), River hydraulics, sediment transport and training works: their ecological relevance to European rivers, Archiv. Hydrobiol. Suppl., Vol. 113, No. 10, pp. 129-146.

Copeland, R. R. (1983), Bank protection techniques using spur dikes, Miscellaneous Paper HL-83-1, U. S. Army Engineer Waterways Experiment Station, Vicksburg, Miss.

Gill, M.A. (1972), Erosion of sands beds around spur dikes, Journal of Hydraulic Division, ASCE, Vol. 98, No. 9, pp. 1587-1602.

Klaassen, G. J., Douben, K. and van der Waal, M. (2002), Novel approaches in river engineering, River flow 2002, Bousmar & Zech, eds., Swets & Zeitlinger, Lisse, pp. 27-42.

Klingeman, P. C., Kehe, S. M. and Owusu, Y. A. (1984), Streambank erosion protection and channel scour manipulation using rockfill dikes and gabions, Rep. No. WRRI-98, Water Resources Research Institute, Oregon State University, Corvallis, Oregon.

Kuhnle et al. (2002), Local scour associated with angled spur dikes, ASCE, Journal of Hydraulic Engineering, vol. 128, No. 12.

Maza Alvarez, J.A. (1990), Contribuicion al diseno de espigones, in XIV Congresso Latino Americano de Hidraulica, Montevideo.

Rodi, W. (1980), Turbulence models and their application in hydraulics- a state of art review, University of Karlsruhe , Germany.

Uijttewaal, W.S.J. (2005), Effects of groin layout on the flow in groin fields: laboratory experimental, Journal Hydraulic Engineering, ASCE, Vol. 131, No. 9, pp. 782-791.

Zhang, H. (2005), Study on Flow and Bed Evolution in Channels with Spur Dykes, Doctoral Dissertation, Kyoto University.

Zhang, H., Nakagawa, H., Muto, Y., Touchi, D. and Muramoto, Y. (2006a), 2D numerical model for river flow and bed evolution based on unstructured mesh, Journal of Applied Mechanics, JSCE, vol. 9, pp. 783-794.

Zhang, H., Nakagawa, H., Muto, Y., Baba, Y. and Ishigaki, T. (2006b), Numerical simulation of flow and local scour around hydraulic structures, River flow 2006, pp. 1683-1693.